CD44 Interacts with HIF-2 to Modulate the Hypoxic Phenotype of Perinecrotic and Perivascular Glioma Cells

Johansson, Elinn; Grassi, Elisa S.; Pantazopoulou, Vasiliki; Tong, Bei; Lindgren, David; Berg, Tracy J.; Pietras, Elin J.; Axelson, Håkan; Pietras, Alexander

Published in:
Cell Reports

DOI:
10.1016/j.celrep.2017.07.049

Publication date:
2017

Document version
Publisher's PDF, also known as Version of record

Article

Cell Reports

CD44 Interacts with HIF-2α to Modulate the Hypoxic Phenotype of Perinecrotic and Perivascular Glioma Cells

Graphical Abstract

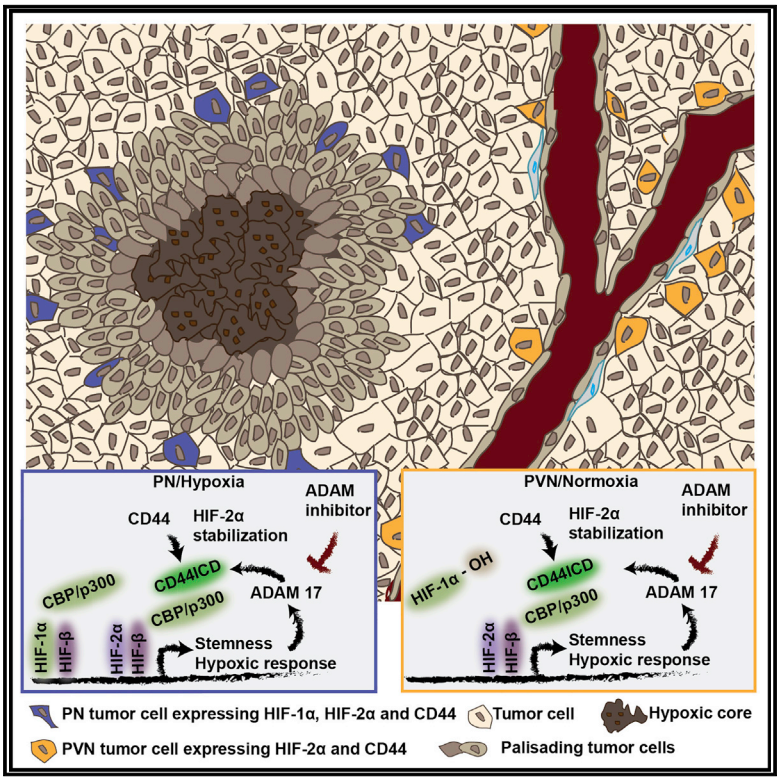

Highlights

- CD44 cleavage to release the CD44ICD is enhanced at hypoxia in glioma
- The CD44 ICD enhances HIF-dependent hypoxic and pseudo-hypoxic signaling
- The CD44 ICD interacts directly with HIF-2α, but not HIF-1α
- Blocking CD44 cleavage reduces hypoxia-induced glioma stemness

Authors

Elinn Johansson, Elisa S. Grassi, Vasiliki Pantazopoulou, ..., Elin J. Pietras, Håkan Axelson, Alexander Pietras

Correspondence

alexander.pietras@med.lu.se

In Brief

Hypoxia-inducible factors (HIFs) maintain glioma stemness, and stem-like glioma cells have an amplified hypoxic response compared to bulk tumor cells. Johansson et al. show that the glioma stem cell marker CD44 is activated under hypoxia and interacts with HIF-2α to enhance the hypoxic and pseudo-hypoxic phenotype of glioma stem cells.

Johansson et al., 2017, Cell Reports *20*, 1641–1653
August 15, 2017
http://dx.doi.org/10.1016/j.celrep.2017.07.049

CellPress

Cell Reports
Article

CD44 Interacts with HIF-2α to Modulate the Hypoxic Phenotype of Perinecrotic and Perivascular Glioma Cells

Elinn Johansson,[1] Elisa S. Grassi,[1] Vasiliki Pantazopoulou,[1] Bei Tong,[1] David Lindgren,[1] Tracy J. Berg,[1] Elin J. Pietras,[2] Håkan Axelson,[1] and Alexander Pietras[1,3,*]

[1]Division of Translational Cancer Research, Department of Laboratory Medicine, Lund University, Scheelevägen 2, Medicon Village 404:C3, 223 63 Lund, Sweden

[2]Biotech Research and Innovation Centre, University of Copenhagen, Copenhagen 2200, Denmark

[3]Lead Contact

*Correspondence: alexander.pietras@med.lu.se

http://dx.doi.org/10.1016/j.celrep.2017.07.049

SUMMARY

Hypoxia-inducible factors enhance glioma stemness, and glioma stem cells have an amplified hypoxic response despite residing within a perivascular niche. Still, little is known about differential HIF regulation in stem versus bulk glioma cells. We show that the intracellular domain of stem cell marker CD44 (CD44ICD) is released at hypoxia, binds HIF-2α (but not HIF-1α), enhances HIF target gene activation, and is required for hypoxia-induced stemness in glioma. In a glioma mouse model, CD44 was restricted to hypoxic and perivascular tumor regions, and in human glioma, a hypoxia signature correlated with *CD44*. The CD44ICD was sufficient to induce hypoxic signaling at perivascular oxygen tensions, and blocking CD44 cleavage decreased HIF-2α stabilization in CD44-expressing cells. Our data indicate that the stem cell marker CD44 modulates the hypoxic response of glioma cells and that the pseudo-hypoxic phenotype of stem-like glioma cells is achieved by stabilization of HIF-2α through interaction with CD44, independently of oxygen.

INTRODUCTION

Glioblastoma multiforme (GBM), the highest-grade glioma and deadliest brain tumor, responds well to surgery and irradiation but invariably recurs as incurable treatment-resistant disease (Huse and Holland, 2010). Resistance has been linked to the presence of stem-like tumor cells located primarily in a perivascular niche (PVN) (Hambardzumyan and Bergers, 2015), identified by expression of stem cell markers like CD133 (Singh et al., 2003) or CD44 (Anido et al., 2010). Few viable strategies targeting such stem-like glioma cells have been identified, in part because most known drivers of stemness are essentially non-druggable transcription factors like the hypoxia-inducible factors (HIFs).

Solid tumors frequently develop areas of hypoxia due in part to tumors outgrowing the vascular supply and in part to tumor vasculature malfunctioning (Semenza, 2012). This is particularly true for GBMs, as one hallmark pathognomonic feature of GBMs is pseudopalisading necrosis with surrounding hypoxia (Huse and Holland, 2010). The cellular response to hypoxia is primarily driven by two transcription factors: the oxygen-regulated HIF-1α and HIF-2α. The HIFs regulate numerous pathways and processes, including angiogenesis and a metabolic switch toward anaerobic glycolysis (Semenza, 2012). In tumors, the hypoxic response frequently also induces dedifferentiation of tumor cells toward stem-like states. HIF expression has been linked to enhanced stemness in glioma, and glioma stem cells display an amplified hypoxic response, sometimes despite a perivascular localization (Bar et al., 2010; Heddleston et al., 2009; Li et al., 2009; Seidel et al., 2010; Soeda et al., 2009). While HIF-1α and HIF-2α share regulation by oxygen and the majority of target genes, it appears that HIF-2α is the primary driver of this hypoxia-induced dedifferentiation, as well as of pseudo-hypoxic phenotypes of apparently well-vascularized stem-like glioma cells (Pietras et al., 2010). Little is known about the differential regulation of HIF-α subunits in stem-like versus tumor bulk cells in glioma and other solid tumor types.

We previously found that the stem cell marker CD44 is specifically expressed in the PVN of proneural GBM and that its cleavage by gamma-secretase can release an intracellular domain (CD44ICD) capable of enhancing target gene activation by HIFs (Pietras et al., 2014). Here, we investigate the role of CD44 in regulation of hypoxic and pseudo-hypoxic phenotypes of human and murine glioma cells. We demonstrate that CD44 cleavage is enhanced at hypoxia and that pharmacological inhibition of this cleavage attenuates the hypoxic response. Inhibition of CD44 cleavage resulted in decreased HIF-2α, but not HIF-1α, levels at hypoxia, and CD44ICD interacted specifically with HIF-2α, resulting in enhanced HIF target activation at both hypoxic and perivascular oxygen tensions. In murine GBM in vivo, CD44 was specifically located in a perivascular, well-oxygenated niche characterized by pseudo-hypoxic, HIF-2α-positive, stem-like cells, as well as in a perinecrotic, hypoxic niche characterized by HIF-1α- and HIF-2α-positive glioma cells. Expression of *CD44* and enzymes responsible for CD44ICD generation correlated positively with a hypoxia gene signature in the human GBM The Cancer Genome Atlas (TCGA) dataset, and inhibition of CD44 cleavage diminished hypoxia-induced stem cell characteristics and induced differentiation of primary

glioma cells. Our data highlight differential regulation of HIF-α subunits in stem-like tumor cells.

RESULTS

CD44 Expression and Cleavage Is Enhanced at Hypoxia in Glioma

High-grade gliomas were generated using the RCAS/tv-a system to express *PDGFB* and small hairpin RNA (shRNA) targeting *Tp53* in nestin-expressing cells of neonatal *Ntv-a Ink4a/Arf*$^{-/-}$ mice (Holland et al., 1998; Shih et al., 2004). Tumors were stained for CD44 and the neural stem cell marker nestin to identify stem-like GBM cells and the PVN in vivo. As previously reported (Pietras et al., 2014), CD44 staining was intensely present in the PVN, where CD44 and nestin expression overlapped (Figure 1A). Interestingly, while the bulk of the tumor was negative for CD44 staining, CD44 was also specifically enriched in hypoxic, CAIX-expressing, perinecrotic (PN) cells, indicating that CD44 regulation of hypoxic signaling could occur in vivo (Figure 1A). *PDGFB*-induced glioma primary cultures (PIGPCs) were isolated from tumors and subjected to culture under normoxic (21% oxygen [O_2]) or hypoxic (1% O_2) conditions. CD44ICD is generated from full-length CD44 in a two-step cleavage process mediated by ADAM10/17 (to generate the membrane-bound COOH-terminal fragment of CD44 [CD44EXT]), then gamma-secretase (to generate CD44ICD) (Nagano and Saya, 2004). CD44ICD generation was significantly enhanced by hypoxia in PIGPCs (Figure 1B). Similarly, CD44EXT and CD44ICD levels were both increased in human U251MG glioma cells cultured at hypoxia (Figure 1C), whereas full-length CD44 protein and *CD44* mRNA levels were largely unaffected by hypoxia in both human and murine glioma cells (Figures 1B, 1C, S1A, and S1B). Band identities were confirmed by positive (TPA-induced cleavage) and negative (TPA plus the gamma-secretase inhibitor DAPT to inhibit CD44EXT-to-ICD cleavage) controls (Figure 1C). The marked increase in CD44EXT following gamma-secretase inhibition suggests that CD44ICD generation is underestimated by quantifying the band corresponding to CD44ICD, likely due to the short half-life of gamma-secretase-generated ICDs (Figure 1C).

To confirm the increase in intracellular CD44 at hypoxia, we stained U251MG cells cultured at normoxia or hypoxia with an antibody recognizing the C-terminal end of CD44. Staining revealed primarily membrane-bound CD44 at normoxia and both membrane-bound and intracellular CD44 at hypoxia (Figure 1D). Quantitative image analysis of fluorescent images confirmed that there was no significant difference in the membrane of cells, but a significant increase in intracellular/cytoplasmic CD44 at hypoxia was found (Figure 1D). Finally, staining *PDGFB*-induced murine gliomas with the C-terminal CD44 antibody revealed an intracellular staining pattern in addition to membrane staining in PN tumor areas (Figure 1E). Together, these data show enhanced CD44 cleavage into CD44ICD and increased intracellular CD44 expression in hypoxic glioma cells in vitro and in vivo.

ADAM17 Expression Is Induced at Hypoxia in Glioma, and ADAM Inhibition Blocks CD44 Cleavage

We speculated that the increased CD44ICD generation at hypoxia could reflect increased activity of the enzymes responsible for cleavage (i.e., ADAM10 and/or ADAM17). Western blot analysis showed increased levels of mature ADAM17, but not ADAM10, protein in hypoxic U251MG cells (Figure 2A). The increased protein levels were associated with a modest but significant increase in ADAM17 (but not ADAM10) mRNA levels after prolonged exposure to hypoxia (Figure 2B). In murine gliomas in vivo, ADAM17 expression was restricted to a subset of cells and overlapped with CD44 expression in hypoxic tumor areas (Figure 2C). In support of these observations, analysis of data from the Allen Institute for Brain Science Ivy Glioblastoma Atlas Project (Ivy GAP) showed significantly higher expression of *ADAM17* in microdissected PN tumor areas than in tumor bulk (Figure 2D; $p < 0.01$, Tukey's HSD test). To test whether the induction of *ADAM17* at hypoxia was dependent on HIFs, we used small interfering RNA (siRNA) to knock down *HIF1A* and *HIF2A*, respectively, in U3065MG cells cultured at hypoxia. Targeting *HIF2A*, but not *HIF1A*, significantly diminished the hypoxic induction of mature ADAM17 protein (Figure 2E). Finally, to test whether ADAMs were indeed responsible for CD44 cleavage, we employed three structurally independent pharmacological inhibitors of ADAM activity: TAPI-2, TMI 1, and GI 254023X. All three inhibitors reduced CD44EXT levels (Figure 2F), suggesting that induced ADAM17 activity could be responsible for increased CD44ICD levels at hypoxia.

ADAM Inhibition Modulates the Hypoxic Response of Glioma Cells

In light of our recent finding that CD44ICD can signal to enhance HIF activity, our data suggest that CD44 cleavage at hypoxia could represent a mode of tuning the hypoxic response in glioma cells. We used the pharmacological ADAM inhibitors to determine whether CD44ICD release at hypoxia can affect the hypoxic response. Treating PIGPCs, T98G human glioma cells, or U251MG human glioma cells with TAPI-2 indeed resulted in significantly decreased activation of hypoxia responsive elements (HREs) at hypoxia, as measured by luciferase assay (Figures 3A–3C). Furthermore, out of a panel of 9 classical HIF target genes induced by hypoxia in U251MG cells, hypoxic induction of 5 genes (*MXI1*, *BNIP3*, *ADM*, *BHLHE40*, and *NDRG1*) was significantly inhibited by TAPI-2, whereas other genes (*PGK1*, *GLUT1*, *CAIX*, and *VEGF*) were largely unaffected by treatment (Figure 3D). We next performed western blot analysis of HIF-1α and HIF-2α after TAPI-2 treatment of U251MG cells grown at normoxia or hypoxia to test whether the diminished hypoxic response was due to HIF protein level regulation. We found significantly reduced stabilization of HIF-2α, but not HIF-1α, after TAPI-2 treatment, indicating that the reduced HIF activity is mediated by reduced stabilization of HIF-2α (Figure 3E). Similarly, TMI 1 and GI 254023X reduced HIF-2α protein levels at hypoxia (Figure S3). Notably, the Notch intracellular domain, another ADAM10/17-dependent ICD inhibited by TAPI-2, failed to affect HRE activation in glioma cells (Figure S3A), indicating that these effects were unrelated to Notch signaling.

CD44ICD Enhances HIF-2α Specifically via Protein-Protein Interaction

To further elucidate the mechanism underlying HIF-2α stabilization by CD44ICD, we used two inhibitors of the proteasomal HIF

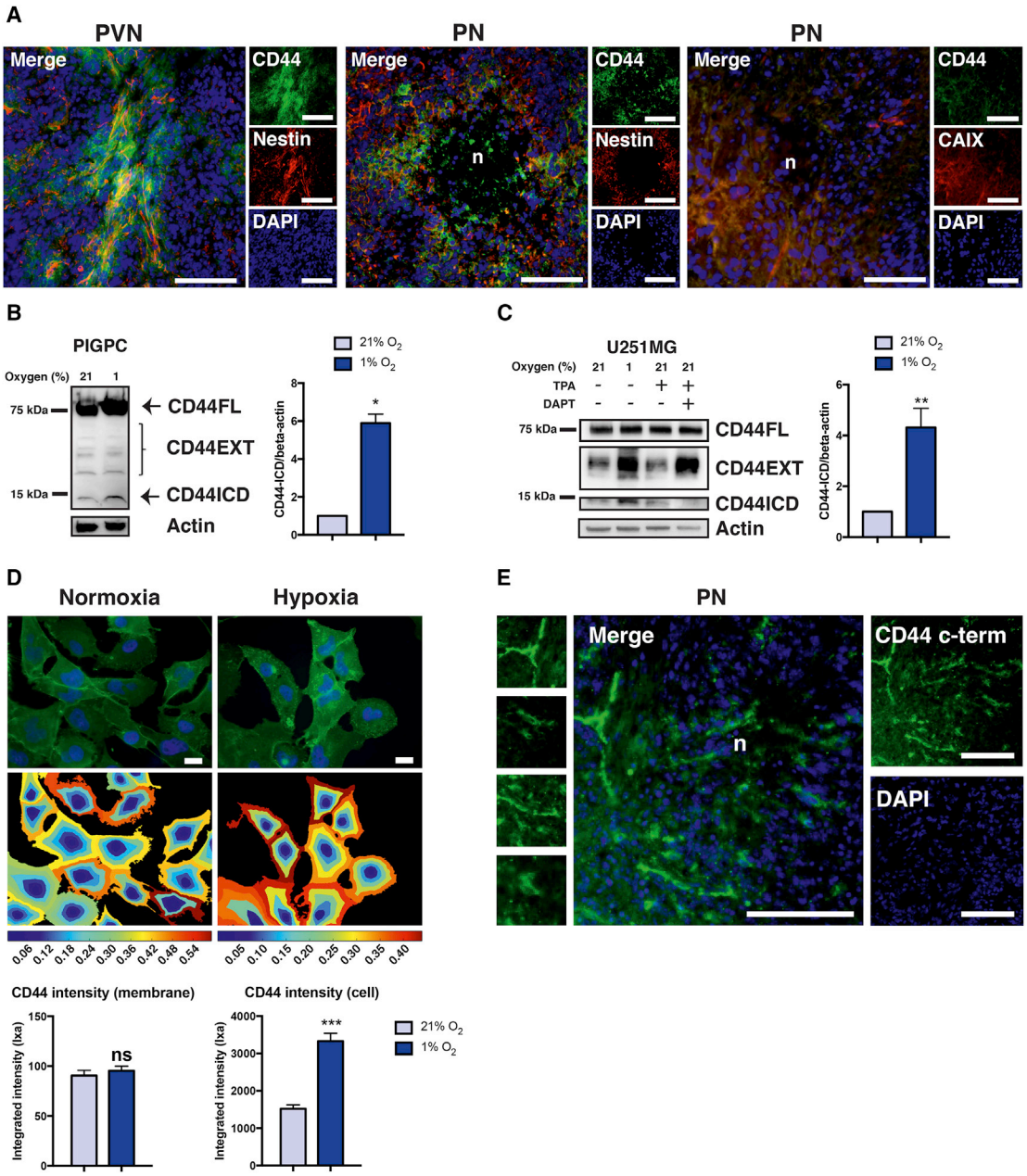

Figure 1. Enhanced Intracellular CD44 at Hypoxia in Glioma In Vivo and In Vitro

(A) Immunofluorescent staining of PDGFB-induced murine gliomas in PVN (left) and PN areas (middle) (CD44, green; nestin, red; DAPI, blue). Immunofluorescence of PN areas (right) (CD44, green; CAIX, red; DAPI, blue). A minimum of 3 regions per tumor from at least 3 independent tumors were analyzed. Scale bars represent 50 μm.

(B and C) Western blot of CD44 and actin in PIGPC (B) and U251MG (C) cells grown for 24 hr at 21% or 1% O_2, treated as indicated with 10 μM DAPT, 200 μM TPA (positive control for CD44ICD), or 200 μM TPA with 10 μM DAPT (negative control for CD44ICD). CD44EXT is CD44 cleaved extracellularly but still membrane bound. Right graph shows quantification of CD44ICD signal across three independent experiments. *$p < 0.05$; **$p < 0.01$ (Student's t test).

(D) Immunofluorescent staining of U251MG cells grown at 21% or 1% O_2 for 24 hr for C-terminal CD44 (green) and DAPI (blue). Scale bars represent 20 μm. Middle panel shows representative pictures of quantification of CD44 staining intensity, where cells are divided into 6 fractions from cell membrane to nucleus. The bottom panel represents CD44 staining intensity in membrane and cell fractions at 21% or 1% O_2, respectively. Data are presented as integrated intensity (IxA). ns, not significant; ***$p < 0.001$ (Student's t test; n = 204 [normoxia], n = 153 [hypoxia]). Data represent one of three independent experiments.

(E) Immunofluorescent staining of PDGFB-induced murine gliomas for C-terminal CD44 (green) and DAPI (blue) in PN tumor areas. A minimum of 3 regions per tumor from at least 3 independent tumors were analyzed. Scale bars represent 50 μm.

In (B)–(D), error bars represent SEM.

See also Figure S1.

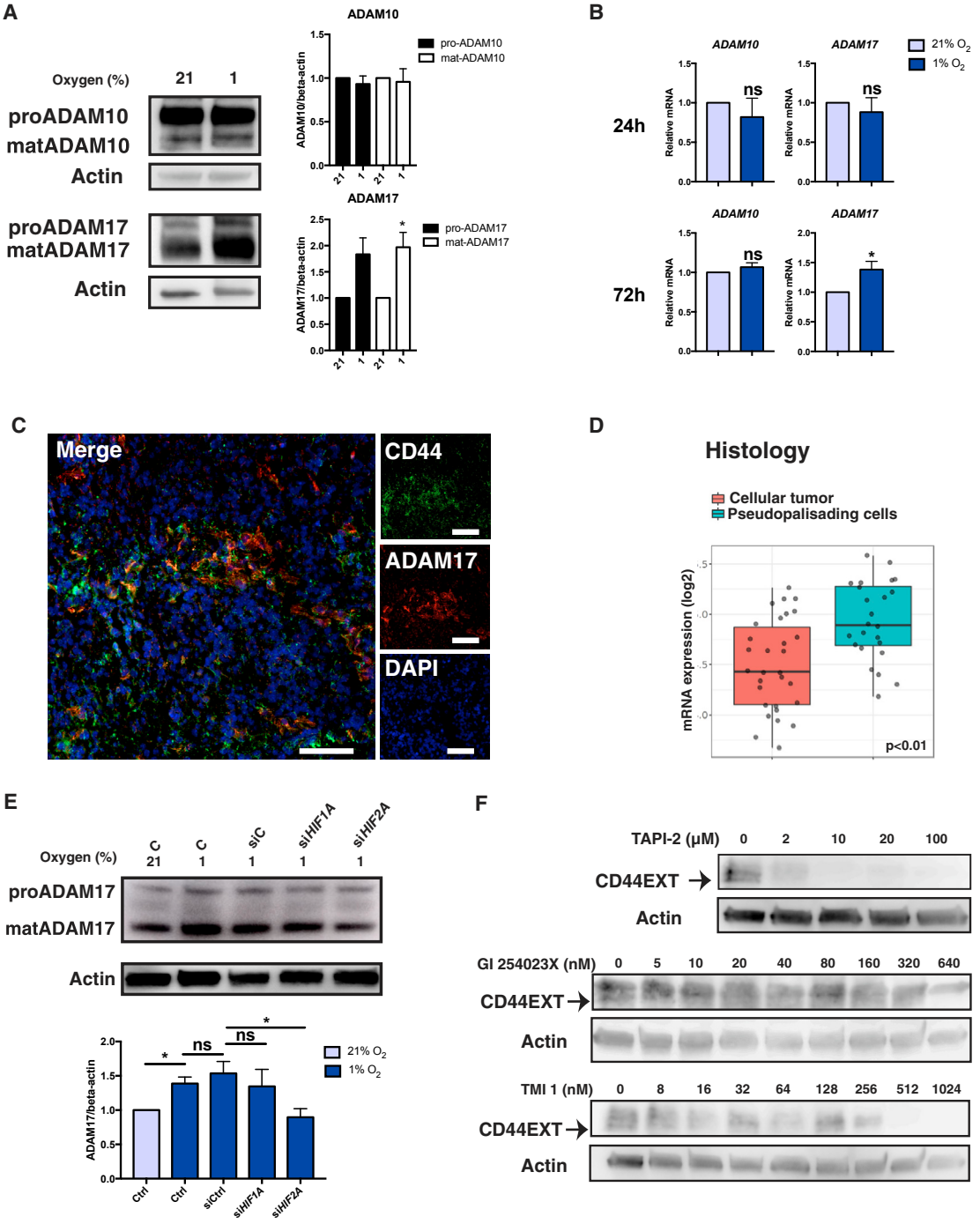

Figure 2. ADAM17 Expression Is Induced at Hypoxia in Glioma, and ADAM Inhibition Blocks CD44 Cleavage

(A) Western blot of ADAM10, ADAM17 (top band, pro-ADAM; bottom band, mature-ADAM) and actin in U251MG cells grown for 24 hr at 21% or 1% O_2. Right graph shows quantification of pro- and mature ADAM10 and ADAM17 signal across three independent experiments. *$p < 0.05$ (Student's t test).

(B) qPCR data for relative mRNA expression of *ADAM10* and *ADAM17* in U251MG cells cultured at 21% or 1% O_2 for the indicated time periods. Data represent mean values from at least three independent experiments. ns, not significant; *$p < 0.05$ (Student's t test).

(C) Immunofluorescent staining of PDGFB-induced murine gliomas (CD44, green; ADAM17, red; DAPI, blue). A minimum of 3 regions per tumor from at least 3 independent tumors were analyzed. Scale bars represent 50 μm.

(D) Relative mRNA expression of *ADAM17* in microdissected pseudopalisading versus cellular tumor cells from the Ivy GAP RNA-sequencing data (Allen Institute for Brain Science Ivy Glioblastoma Atlas Project; http://glioblastoma.alleninstitute.org). $p < 0.01$ (Tukey's honest significant difference).

(legend continued on next page)

degradation pathway. 2,2′-dipyridyl (DIP) inhibits prolyl hydroxylation of HIFs and thereby recognition by von Hippel-Lindau (VHL), and MG132 is a direct proteasome inhibitor. In the presence of either inhibitor, TAPI-2 no longer had any effect on HIF-2α protein levels at hypoxia (Figure 4A), suggesting that ADAM substrates enable HIF-2α to escape the canonical HIF degradation pathway.

We next employed a set of HIF-α mutant constructs (HIF-1 2M, HIF-2 2M, and HIF-1 3M) mutated either at the PHD hydroxylation sites (2M constructs) or at the PHD and factor inhibiting HIF 1 (FIH-1) hydroxylation sites (3M) (Figure 4B). In line with the decreased HIF-2α protein levels in TAPI-2-treated cells (Figure 3E), we found decreased HRE-luciferase activation in TAPI-2 treated cells transfected to express an O_2-insensitive HIF-2α, but not HIF-1α (Figure 4C). Similarly, CD44ICD overexpression significantly enhanced HRE-luciferase activity of cells expressing HIF-2 2M, but not HIF-1 2M (Figure 4D). As this potentiation of HRE activation by CD44ICD was previously found to be dependent on CREB-binding protein (CBP)/p300 (Pietras et al., 2014), and as HIF-2α is less sensitive to FIH-mediated hydroxylation than HIF-1α (Bracken et al., 2006; Yan et al., 2007), we tested whether a HIF-1α mutant insensitive to FIH-mediated hydroxylation (and thus FIH-mediated inhibition of HIF-1α/CBP/p300 interactions at normoxia) (HIF-1 3M) would mimic the results of HIF-2α overexpression. Strikingly, HIF-1 3M displayed the same enhanced HRE activation by CD44ICD as HIF-2 2M (Figure 4D). We next performed co-immunoprecipitation using these HIF-α constructs together with an EGFP-CD44ICD construct in cultured U251MG glioma cells. Interestingly, EGFP-CD44ICD interacted directly with HIF-2 2M, but not HIF-1 2M, as demonstrated by immunoprecipitating both hemagglutinin (HA) (for the HIF constructs) and EGFP (for CD44ICD) (Figure 4E). Again, HIF-1 3M could mimic the effects of HIF-2 2M and bound directly to CD44ICD (Figure 4E). To further test the involvement of FIH-1 in the differential regulation of HIF-1α versus HIF-2α by CD44, we used siRNA to knock down FIH-1 expression. Interestingly, both HIF-1 2M and HIF-2 2M constructs were able to bind CD44ICD in cells with FIH-1 levels knocked down, whereas only HIF-2 2M was able to bind in siControl transfected cells (Figure 4F). These data demonstrate differential regulation of HIF-1α versus HIF-2α specifically in CD44-expressing tumor cells and highlight FIH-1 as a central factor in differential regulation of HIF-1α versus HIF-2α.

CD44 Is Associated with Hypoxic and Pseudo-Hypoxic GBM Phenotypes

We next co-stained murine PDGFB-induced GBM tumors for CD44 and HIF-1/2α. HIF-1α expression overlapped with CD44 in PN tumor areas but was undetectable in the PVN (Figure 5A). HIF-2α expression overlapped entirely with CD44 expression, with intense staining both in the hypoxic PN and well-vascularized PVN areas (Figure 5B). These data suggest that CD44 can contribute to a pseudo-hypoxic phenotype of stem-like PVN glioma cells by interacting with and stabilizing HIF-2α. To test this hypothesis, we cultured U251MG cells at 21% O_2 (normoxia) or 5% O_2 (an estimation of the physiological PVN O_2 tension), treated or not with TAPI-2 to inhibit CD44 cleavage. Interestingly, HIF-2α protein was stabilized at 5% O_2 and inhibited by TAPI-2 treatment (Figure 5C). Furthermore, CD44ICD overexpression was sufficient to induce significant HRE-dependent luciferase activation in U251MG cells at 5% O_2 (Figure 5D). Together, these data suggest that CD44 expression and activation can enhance hypoxic and pseudo-hypoxic signaling in glioma in vivo at O_2 tensions relevant to both PN and PVN tumor areas.

We next employed a gene signature representative of a classical hypoxic response and applied it to analyze the human GBM dataset from TCGA (Brennan et al., 2013). In line with positive regulation of HIF signaling by CD44ICD, we found a positive correlation between a signature consisting of *CD44*/*ADAM* expression and the hypoxia gene signature ($R = 0.638$; $p < 4.33e^{-19}$) (Figure 5E). Furthermore, dividing tumor samples by GBM subtype revealed that *CD44*/*ADAM* expression largely follows the hypoxia signature, with highest *CD44*/*ADAM* expression as well as hypoxic drive in mesenchymal tumors and lowest expression in G-CIMP tumors (Figure 5F). These data support a role for CD44 cleavage in enhancing hypoxia signaling in human GBM in vivo.

Targeting ADAMs Reduces Glioma Stemness at Hypoxia

We next tested whether pharmacological inhibition of ADAM10/17 could decrease stem cell characteristics of hypoxic glioma cells. First, PIGPCs were subjected to the side population (SP) assay (Bleau et al., 2009; Golebiewska et al., 2013; Wee et al., 2016). The SP of PIGPCs cultured at hypoxia, but not normoxia, was significantly reduced by ADAM inhibition by TAPI-2, TMI 1, or GI 254023X treatment (Figure 6A). We assessed stemness of U251MG cells further by measuring a panel of stem cell marker genes (*NANOG*, *OCT4*, and *SOX2*) by real-time qPCR and found significantly reduced expression of *NANOG*, *OCT4*, and *SOX2* after TAPI-2 treatment of cells grown in hypoxia (Figure 6B). Furthermore, we assessed self-renewal by sphere formation in human primary GBM U3065MG cells from the Human Glioblastoma Cell Culture Resource (HGCC) project (Xie et al., 2015) and found that blocking ADAM10/17 activity affected the size of the spheres; TAPI-2-treated spheres were significantly smaller than control spheres (Figure 6C). TAPI-2 treatment did not affect cell proliferation under adherent conditions (Figure S3). To directly test the involvement of CD44 in the response to ADAM inhibition in stemness, we set up the same sphere-formation experiment in U3065MG cells treated with control or siRNA

(E) Western blot of ADAM17 and actin in U3065MG cells grown for 24 hr at 21% or 1% O_2 expressing control, non-targeting siRNA or siRNA targeting *HIF1A* and *HIF2A*, respectively. Bottom panel shows quantification of the ADAM17 signal across three independent experiments. ns, not significant; *$p < 0.05$ (Student's t test).

(F) Western blot of CD44 and actin in U251MG cells treated for 24 hr as indicated with TAPI-2 (top), GI 254023X (middle), or TMI 1 (bottom). Data show one representative experiment out of three independent experiments.

In (A), (B), (D), and (E), error bars represent SEM.

See also Figure S2.

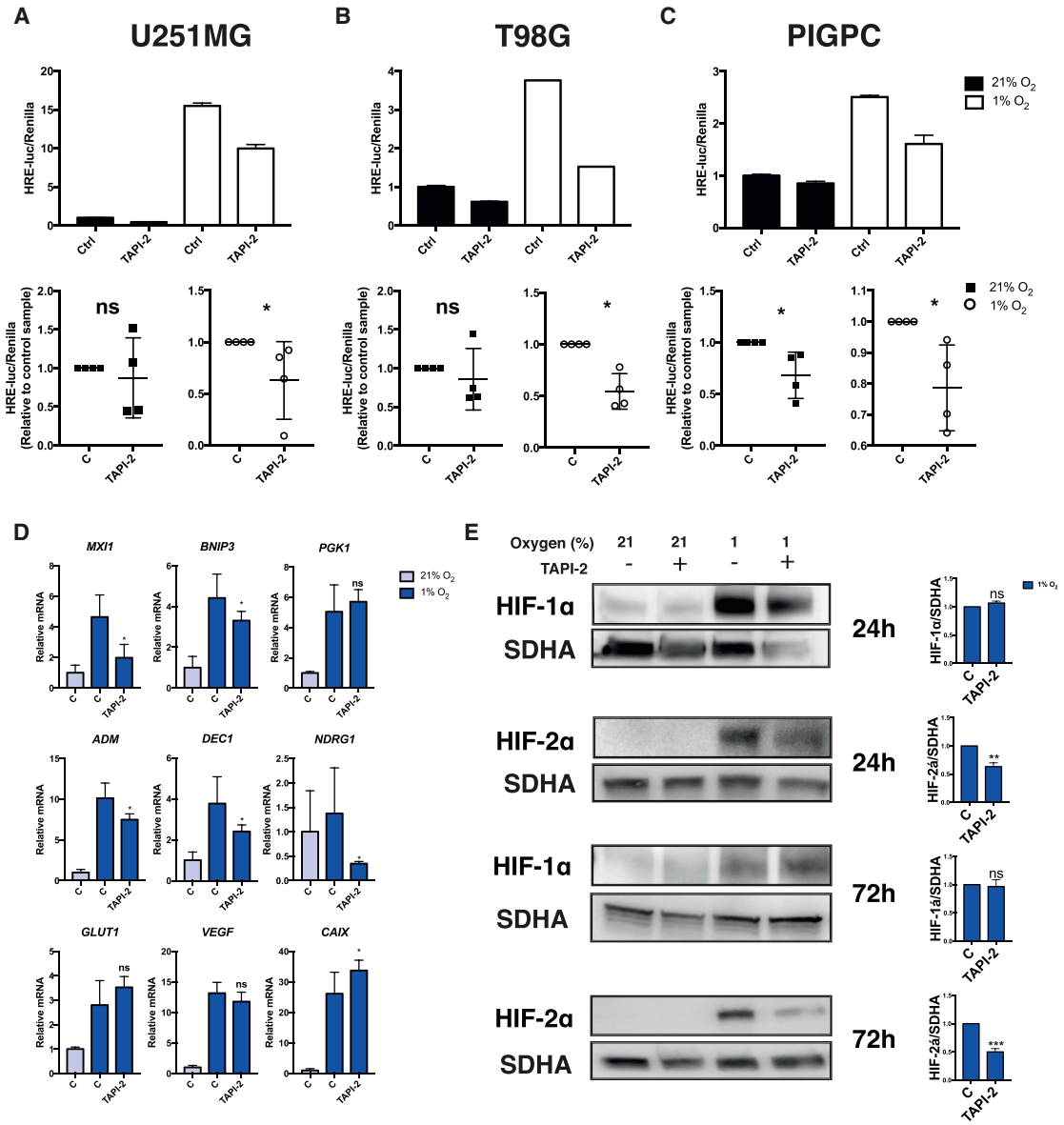

Figure 3. ADAM Inhibition Modulates the Hypoxic Response by Regulating HIF-2α, but Not HIF-1α

(A–C) HRE-luciferase normalized to Renilla for U251MG (A), T98G (B), and PIGPC (C) cells pre-treated with 20 μM TAPI-2 for 24 hr following 48-hr treatment at 21% or 1% O_2. Top graphs represent one representative experiment, and error bars represent SD. Bottom graphs represent data normalized to control from four independent experiments, and error bars represent SEM. *p < 0.05; ns, not significant (Mann-Whitney test).

(D) qPCR data for relative mRNA expression of *MXI1*, *BNIP3*, *PGK1*, *GLUT1*, *ADM*, *BHLHE40 NDRG1*, and *VEGF* in U251MG cells treated with 20 μM TAPI-2 and cultured at 21% or 1% O_2. Data represent mean values from at least three independent experiments. *p < 0.05; ns, not significant (Student's t test).

(E) Western blot analysis of HIF-1α, HIF-2α, and SDHA in U251MG cells grown at 21% or 1% O_2 for 24 hr or 72 hr, treated with 20 μM TAPI-2. Right panel shows quantification of HIF-1α and HIF-2α signal across three independent experiments. ns, not significant; **p < 0.01; ***p < 0.01 (Student's t test).

In (D) and (E), error bars represent SEM.

See also Figure S3.

targeting *CD44*. In agreement with TAPI-2 treatment acting through inhibition of CD44 cleavage, data showed that *CD44* knockdown reduced sphere size to a similar degree as TAPI-2 treatment of control or control siRNA-treated cells (Figure 6D). Most importantly, TAPI-2 treatment could not further reduce sphere size in cells lacking *CD44* expression (Figure 6D), strongly suggesting that TAPI-2-mediated effects are dependent on inhibition of CD44 cleavage.

We finally extended our analysis to include primary glioma cultures from different molecular subtypes: U3035 and U3065 (both mesenchymal), U3082 (proneural), and U3084 (classical) (Xie et al., 2015). As expected from bioinformatic analyses

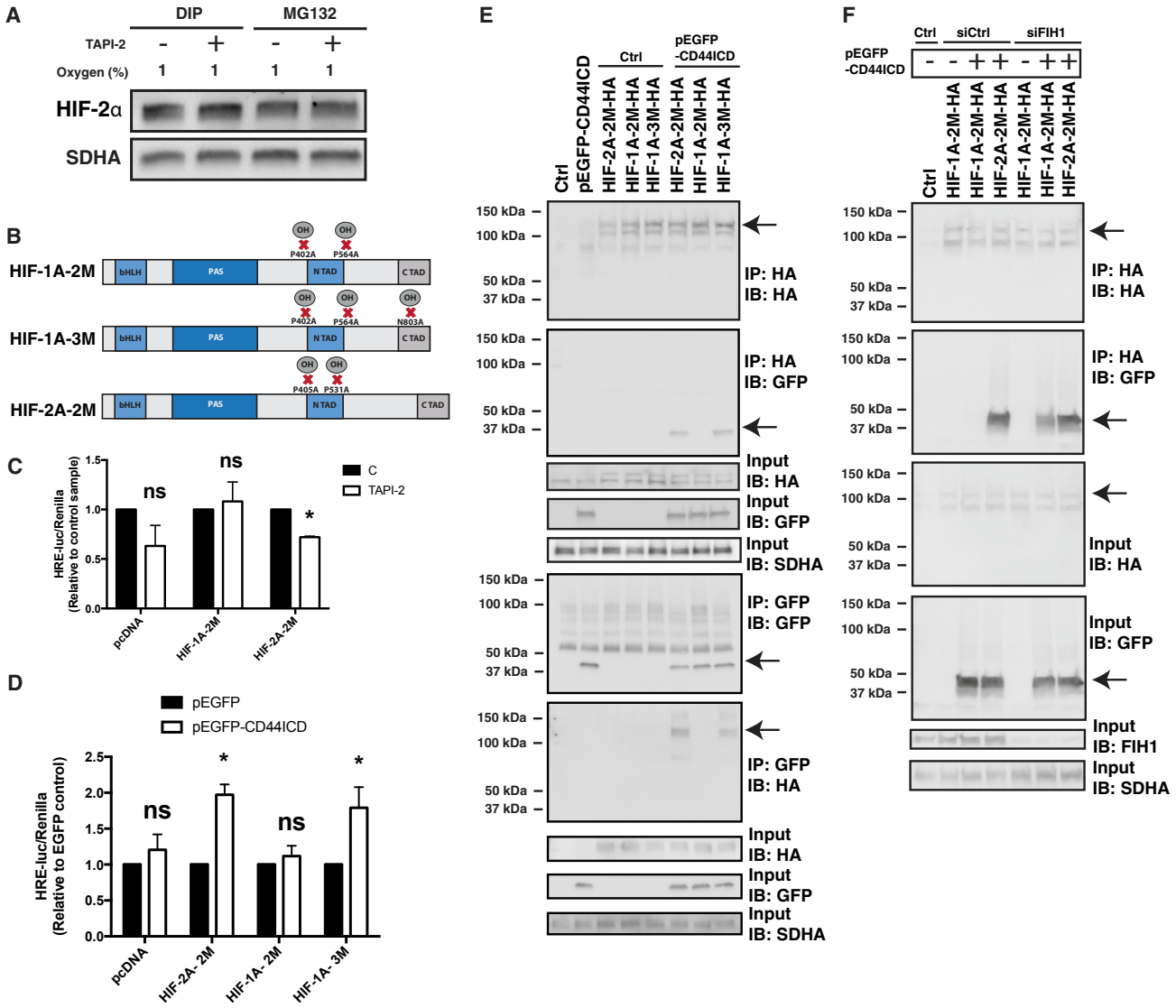

Figure 4. CD44ICD Interacts Specifically with HIF-2α, but Not HIF-1α

(A) Western blot analysis of HIF-2α and SDHA in U251MG cells grown at 1% O_2 for 24 hr, treated as indicated with 20 μM TAPI-2, 200 μM DIP, and 10 μM MG132. Data show one representative experiment out of three independent experiments.

(B) Schematic of the HIF mutants used in the study. The basic-helix-loop-helix (bHLH), Per-Arnt-Sim (PAS), N-terminal transactivation domain (NTAD), and C-terminal transactivation domain (CTAD) are indicated by boxes. The Pro402-to-Ala, Pro564-to-Ala, Pro405-to-Ala, Pro531-to-Ala, and Asn813-to-Ala substitutions are indicated.

(C) HRE-luciferase normalized to Renilla for T98G cells pretreated 24 hr with 20 μM TAPI-2 expressing pCDNA control, pCDNAHIF-1A-2M, or pCDNAHIF-2A-2M. Data represent mean values from at least three independent experiments and are normalized to control. *$p < 0.05$; ns, not significant (Mann-Whitney test).

(D) HRE-luciferase normalized to Renilla for U251MG cells expressing pEGFP control or pEGFP-CD44ICD together with pCDNA control, pCDNAHIF-1A-2M, pCDNAHIF-1A-3M, or pCDNAHIF-2A-2M. Data represent mean values from at least three independent experiments and are normalized to pEGFP control. *$p < 0.05$; ns, not significant (Mann-Whitney test).

(E) Co-immunoprecipitation of EGFP-CD44ICD together with HA-tagged pCDNAHIF-1A-2M, pCDNAHIF-1A-3M, or pCDNAHIF-2A-2M in U251MG cells. Data show one representative experiment out of three independent experiments.

(F) Co-immunoprecipitation of EGFP-CD44ICD together with HA-tagged pCDNAHIF-1A-2M or pCDNAHIF-2A-2M in U251MG cells expressing siRNA targeting control or *HIF1AN* (gene encoding FIH-1) as indicated. Data show one representative experiment out of three independent experiments.

In (C) and (D), error bars represent SEM.

(Figure 5F), the two mesenchymal lines displayed higher basal CD44 protein levels than the proneural and classical lines (Figure 7A). We tested whether the decrease in stem cell characteristics by ADAM inhibition (Figure 6) was accompanied by induction of neuronal and/or astrocytic differentiation. All four primary cultures responded to some extent to ADAM inhibition with

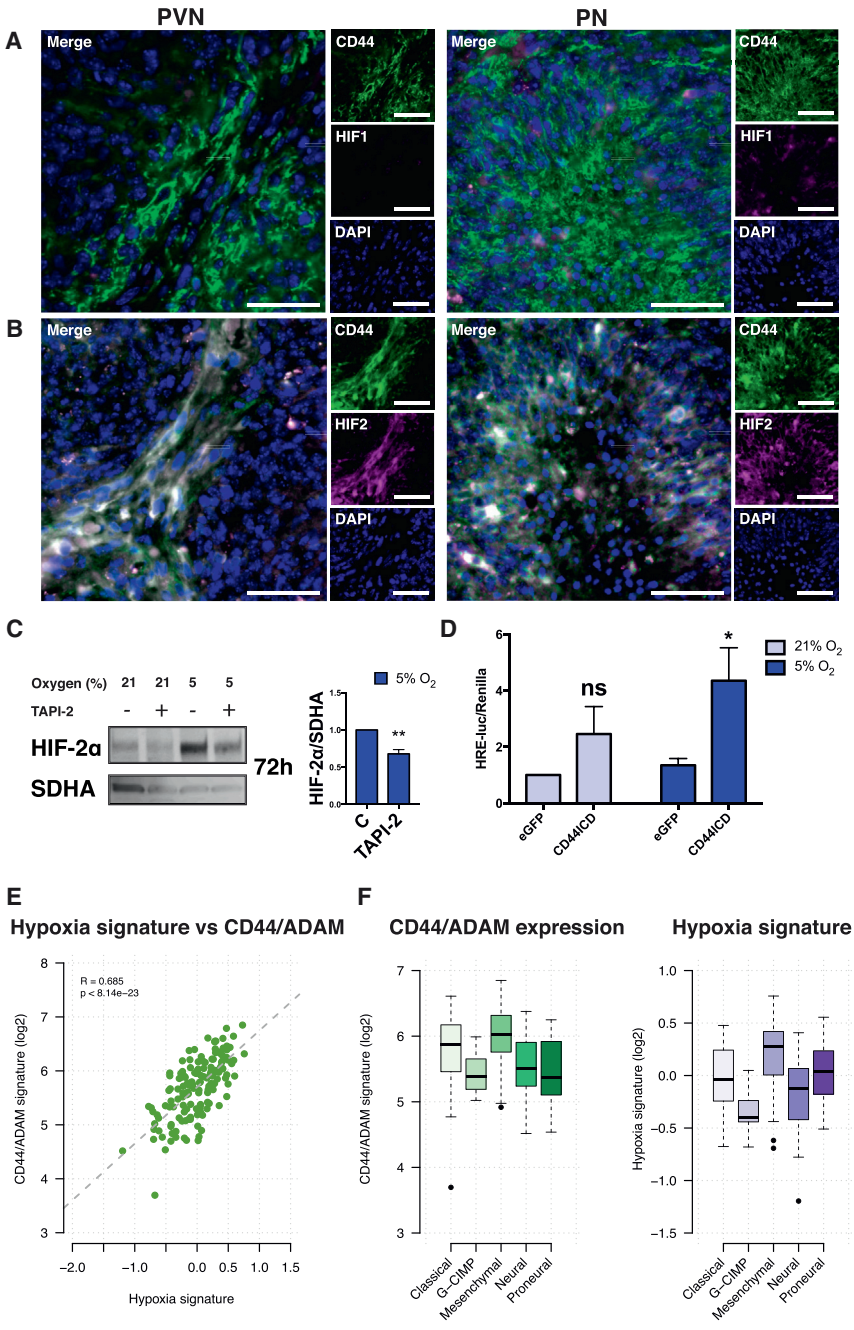

Figure 5. CD44 Modulates Hypoxic and Pseudo-Hypoxic Phenotypes in GBM In Vivo

(A and B) Immunofluorescence of PDGFB-induced murine gliomas in PVN (left) and PN areas (right) (CD44, green; HIF1, magenta [A]; HIF2, magenta [B]; DAPI, blue). A minimum of 3 regions per tumor from at least 3 independent tumors were analyzed. Scale bars represent 50 μm.

(C) Western blot of HIF-2α and SDHA in U251MG cells grown for 72 hr at 21% or 5% O_2 and treated with 20 μM TAPI-2. Right panel shows quantification of HIF-2α signal across three independent experiments HIF-2α. **$p < 0.01$ (Student's t test).

(D) HRE-luciferase normalized to Renilla for U251MG cells expressing pEGFP control or pEGFP-CD44ICD at 21% or 5% O_2. Data represent mean values from three independent experiments. ns, not significant; *$p < 0.05$ (Student's t test).

(E) Scatterplot of hypoxic signature score (x axis) against gene expression levels of *CD44/ADAM* signature score (y axis) in 155 glioblastoma samples from TCGA repository. Pearson correlation coefficients (R) and p values are provided.

(F) Boxplots of *CD44/ADAM* expression (left) and expression of hypoxic signature score (right) in glioblastomas stratified by molecular subclass: classical (n = 40), G-CIMP (n = 8), mesenchymal (n = 49), neural (n = 26), and proneural (n = 31).

In (C) and (D), error bars represent SEM.

significantly increased protein levels of astrocytic (GFAP) or neuronal (Tuj1) markers at hypoxia (Figure 7B). Notably, the two mesenchymal lines with the highest CD44 expression displayed a stronger induction of both differentiation markers than the proneural and classical line (Figure 7B).

DISCUSSION

Differential regulation of HIF-1α versus HIF-2α by O_2 and time has been previously reported (Holmquist-Mengelbier et al., 2006), as well as apparent differential regulation of HIFs in stem-like versus bulk tumor cells (Heddleston et al., 2009; Li et al., 2009). Nevertheless, relatively few underlying molecular mechanisms have been described. Any model of differential HIF regulation in GBM in vivo must take into account that O_2 levels alone cannot sufficiently explain the observed expression patterns described here, as HIF-2α is expressed in the most (PVN) and least (PN) oxygenated tumor areas, but not in tumor bulk (HIF-1α is expressed only in PN areas). One key molecular difference between these HIF-α subunits is the differential sensitivity to FIH-1-mediated asparagine hydroxylation; HIF-1α is significantly more sensitive to this modification than HIF-2α (Bracken et al., 2006; Yan et al., 2007). Hydroxylation by FIH inhibits HIF-α binding to its co-factors CBP and p300, representing an additional layer of O_2-dependent regulation apart from prolyl hydroxylation. We and others have previously demonstrated that CD44ICD-mediated transcriptional effects are dependent on CBP and p300 (Okamoto et al., 2001; Pietras et al., 2014). In light of these data, we speculated that the differential regulation of HIF-1α versus HIF-2α by CD44ICD was dependent on FIH-mediated hydroxylation. This could be of particular interest, as HIF-2α, but not HIF-1α, is stabilized specifically in the non-hypoxic PVN, where FIH-mediated hydroxylation would be involved in HIF

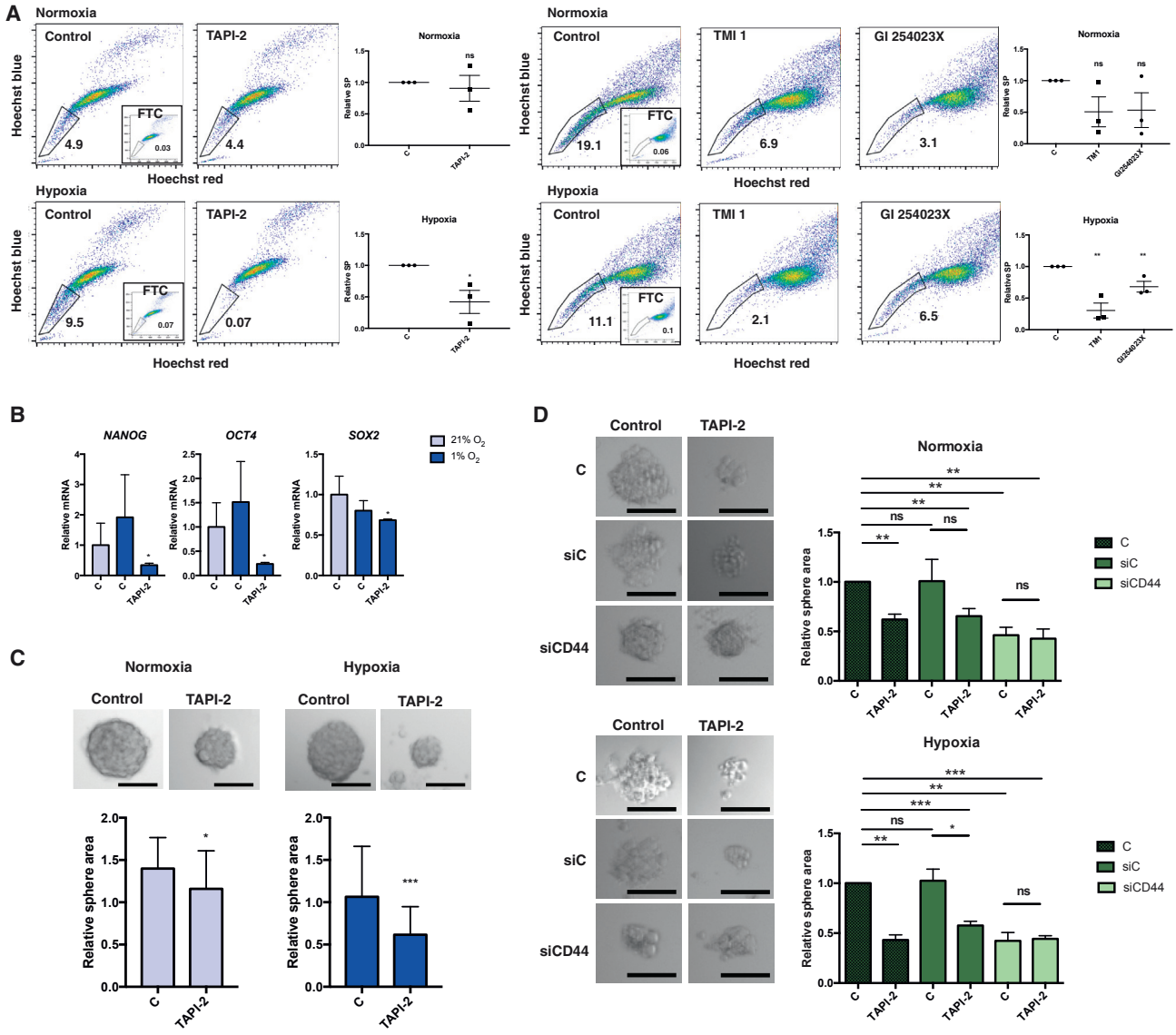

Figure 6. ADAM Inhibition Blocks Stemness in Hypoxic Glioma Cells

(A) Side population assay of PIGPC cells pretreated with 20 μM TAPI-2, 0.5 μM TMI1, and 1 μM GI 254023X, respectively, grown at 21 or 1% O_2 for 48 hr. Right graphs show quantification across three independent experiments. *$p < 0.05$, **$p < 0.01$; ns, not significant (Student's t test).

(B) qPCR data for relative mRNA expression of *NANOG*, *OCT4*, and *SOX2* in U251MG cells treated with 20 μM TAPI-2 and grown in 21% or 1% O_2. Data represent mean values from at least three independent experiments. *$p < 0.05$; ns, not significant (Student's t test).

(C) Sphere-formation assay with U3065MG cells treated with 20 μM TAPI-2 at 21% or 1% O_2. Bottom panel shows quantification of relative sphere area from three independent experiments. Scale bars represent 100 μm, and error bars represent SEM. *$p < 0.05$, ***$p < 0.001$ (Mann-Whitney test).

(D) Sphere-formation assay with U3065MG cells expressing control or siRNA targeting control or *CD44* treated with 20 μM TAPI-2 at 21% or 1% O_2. Scale bars represent 100 μm. Right panel shows quantification of relative sphere area, where error bars represent SEM. ns, not significant; **$p < 0.01$, ***$p < 0.001$ (Student's t test).

In (A) and (B), error bars represent SEM. See also Figure S4.

regulation. Indeed, we found that the potentiation of HRE-activation by HIF-2α by CD44ICD, as well as the binding of CD44ICD to HIF-2α, could be replicated with HIF-1α if the FIH-hydroxylation site of HIF-1α was mutated or if FIH-1 expression was knocked down. In light of these findings, special care should be taken when interpreting biological data generated with FIH-insensitive HIF-1α mutant constructs.

Our data are consistent with a model where HIF-2α is specifically expressed in the PVN due to the specific expression of the stem cell marker CD44 in the PVN. Since the enhanced HIF activity resulting from CD44ICD expression is dependent on CBP/p300 binding to HIF, this effect is impaired for HIF-1α due to FIH-mediated hydroxylation of PVN HIF-1α (but not HIF-2α) (Figure 7C). These findings have implications for our

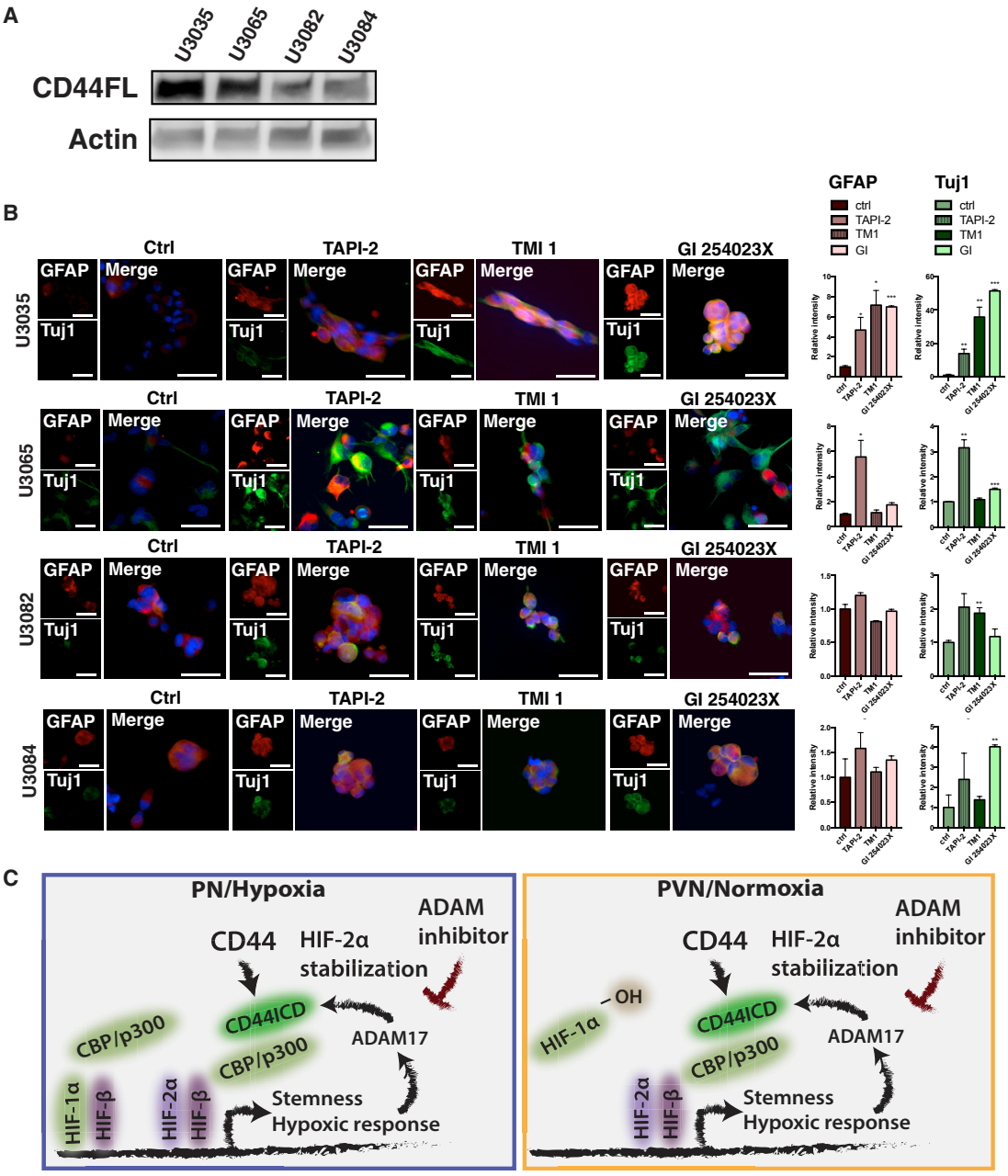

Figure 7. ADAM Inhibition Induces Expression of Differentiation Markers in CD44$^+$ Primary Glioma Cells at Hypoxia

(A) Western blot of CD44 and actin in U3035MG, U3065MG, U3082MG, and U3084MG cells grown at 21% O_2. Data show one representative experiment out of three independent experiments.

(B) Immunofluorescent staining of U3035MG, U3065MG, U3082MG, and U3084MG cells treated with 20 μM TAPI, 0.5 μM TMI 1, or 1 μM GI 254023X and cultured at 1% O_2 for 7 days (GFAP, red; Tuj1, green; DAPI, blue). Scale bars represent 50 μm. Right panel shows quantification of relative intensity of GFAP and Tuj1 staining to control normalized to number of nuclei per field. Data are presented as mean of three independent experiments. Error bars represent SEM. *$p < 0.05$, **$p < 0.01$, ***$p < 0.001$ (Student's t test).

(C) Proposed model of ADAM/CD44-dependent regulation of hypoxic and pseudo-hypoxic glioma phenotypes.

understanding of several observations: Why is HIF-2α expressed at high levels in perivascular and well-oxygenated tumor areas (Holmquist-Mengelbier et al., 2006; Li et al., 2009; Pietras et al., 2014)? Why do stem-like tumor cells have a pseudo-hypoxic phenotype at normoxia and an enhanced hypoxic response at hypoxia (Bar et al., 2010; Li et al., 2009; Pietras et al., 2008, 2010, 2014)? A model where expression and activation of a stem cell marker like CD44 can directly impact HIF-2α stabilization has the potential to explain this differential HIF regulation in stem-like versus bulk glioma cells.

Therapeutic targeting of transcription factors such as HIFs is notoriously difficult, and although both HIF-1α and HIF-2α have been described as prime potential therapeutic targets in many solid tumors, few successful attempts have been reported (Cho and Kaelin, 2016). Our data open for the possibility of targeting HIF-2α specifically in the PVN by targeting the cell-surface-expressed, druggable CD44 receptor. There are several ways in which such inhibition could conceivably work: inhibition of CD44-ligand interactions by blocking antibodies, inhibition of external cleavage of CD44 (as reported here), or inhibition of internal CD44 cleavage using gamma-secretase inhibitors. Our data suggest that stem cell characteristics and parts of the general hypoxic response can be successfully targeted using the approach of targeting ADAM10/17-dependent CD44 cleavage. Further research is warranted to test whether these effects are sufficient to affect treatment resistance of PVN glioma cells.

EXPERIMENTAL PROCEDURES

Generation of Murine Gliomas

Gliomas were induced in *Nestin-tv-a (Ntv-a) Ink4a/Arf*$^{-/-}$ mice by injecting *RCAS-PDGFB* and *RCAS-shp53*-transfected DF-1 cells (ATCC) intracranially in the neonatal brain as previously described (Holland et al., 1998; Ozawa et al., 2014). Mice were monitored daily and euthanized upon symptoms of glioma. All animal procedures were approved by the Malmö-Lund Ethical Committee (permit M186-14), and the use of laboratory animals was conducted in accordance with European Union directive on the subject of animal rights.

Immunofluorescence

Cryosections from *PDGFB*-induced murine gliomas were fixed in acetone and permeabilized in PBS containing 0.3% Triton X-100 (Sigma). Sections were blocked for 30 min in serum-free protein block (DAKO, Gostrup, Denmark) and incubated with the following primary antibodies (4°C overnight): HIF-1α (Novus Biologicals NB100-479), HIF-2α (Abcam ab199), CD44 (BD Biosciences 550538), C-terminal CD44 (Abcam ab157107), nestin (BD Biosciences 556309), HIF-1α (Novus Biologicals NB100-479), HIF-2α (Abcam ab199, Dako), CAIX (R&D Systems AF2344), ADAM17 (LSbio LS-B619-50), Tuj1 (BioLegend 801201) or GFAP (Dako Z0334) (diluted in antibody diluent with Background Reducing Components; DAKO, Gostrup, Denmark) followed by washing and incubation with EnVision FLEX MOUSE (linker) DM824 combined with subsequent incubation with mouse immunoglobulin G (IgG) made in rabbit 1:600 (ab125907) in antibody diluent (DM830, DAKO), or EnVision FLEX RABBIT (linker DM825, DAKO). After washing, sections were incubated with Alexa Fluorchrome 488 and 546 (Invitrogen) followed by washing and mounting in Vechtashield Hard Set with DAPI (Vector Laboratories, Burlingame, CA). Images were acquired using an Olympus BX63 microscope and DP80 camera and cellSens Dimension v 1.12 software (Olympus Corporation).

Quantification of Staining

GFAP and Tuj1 staining was quantified using ImageJ by setting an intensity threshold. Intensity was normalized to the number of nuclei per field. The following list shows the total number of cells analyzed per sample:

U3065MG: 21% O_2, control (Ctrl) n = 1,496; 21% O_2, TAPI-2 n = 140; 21% O_2, GI254023X n = 716; 21% O_2; TMI1 n = 1231; 1% O_2, Ctrl n = 1,084; 1% O_2, TAPI-2 n = 315; 1% O_2, GI254023X n = 779; 1% O_2, TMI1 n = 1,319
U3088MG: 21% O_2, Ctrl n = 770; 21% O_2, TAPI-2 n = 314 ;21% O_2, GI254023X n = 487; 21% O_2, ; TMI1 n = 740; 1% O_2, Ctrl n = 239; 1% O_2, TAPI-2 n = 232; 1% O_2, GI254023X n = 493; 1% O_2, TMI1 n = 239
U3084MG: 21% O_2, Ctrl n = 174; 21% O_2, TAPI-2 n = 131 ;21% O_2, GI254023X n = 92; 21% O_2; TMI1 n = 184; 1% O_2, Ctrl n = 103; 1% O_2, TAPI-2 n = 308; 1% O_2, GI254023X n = 109; 1% O_2, TMI1 n = 198
U3082MG: 21% O_2, Ctrl n = 370; 21% O_2, TAPI-2 n = 601; 21% O_2, GI254023X n = 230; 21% O_2; TMI1 n = 859; 1% O_2, Ctrl n = 167; 1% O_2, TAPI-2 n = 153; 1% O_2, GI254023X n = 430; 1% O_2, TMI1 n = 166
U3035MG: 21% O_2, Ctrl n = 176; 21% O_2, TAPI-2 n = 415; 21% O_2, GI254023X n = 263; 21% O_2; TMI1 n = 332; 1% O_2, Ctrl n = 560; 1% O_2, TAPI-2 n = 405; 1% O_2, GI254023X n = 110; 1% O_2, TMI1 n = 123
U3046MG: 21% O_2, Ctrl n = 489; 21% O_2, TAPI-2 n = 230; 21% O_2, GI254023X n = 482; 21% O_2; TMI1 n = 290; 1% O_2, Ctrl n = 209; 1% O_2, TAPI-2 n = 390; 1% O_2, GI254023X n = 31; 1% O_2, TMI1 n = 167

CD44 C-terminal staining was quantified using CellProfiler (Carpenter et al., 2006) (http://cellprofiler.org). DAPI staining was used for segmentation of nuclei, and CD44 staining was used for segmentation of cells. Intensity for the total cell and for the edge was calculated. Heatmaps were generated illustrating the fraction of the radial distribution of the total stain in each of 6 bins in each cell.

Cell Culture, Hypoxia, and Reagents

PIGPC cells were isolated as previously described (Pietras et al., 2014). U251MG and T98G cells were obtained from ATCC. PIGPC, U251MG, and T98G cells were grown in DMEM (Life Technologies) supplemented with 10% fetal bovine serum (FBS) and 1% PenStrep solution. Hypoxia was generated in Whitney H35 Hypoxiastation (Don Whitley Scientific). Cells were treated with 200 μM DIP (Sigma), 1,6 μM TPA (Sigma), 20 μM TAPI-2 (Sigma), 0.5 μM TMI1 (Tocris Bioscience), and 1 μM GI 254023X (Tocris Bioscience) and 10 μM MG132 (Sigma). Plasmids were transfected using Xtreme gene 9 (Roche) and siRNAs using HiPerFect (QIAGEN) according to the manufacturer's instructions.

siRNAs, non-targeting (D-001810-01-20) *HIF1A* (LQ-004018-00-0002), *HIF2A* (LQ-004814-00-0002), *CD44* (J-009999-07), and *FIH1* (CTM-305836) were from GE Dharmacon. U3035MG, U3065MG, U3082MG, and U3084MG primary glioma cells were obtained from HGCC (http://hgcc.se) and cultured as described previously (Xie et al., 2015) in 1:1 Neurobasal (GIBCO) and DMEM/F12 with Glutamax (Life Technologies) media supplemented with 1% PenStrep, N2, B27 (both from Life Technologies), epidermal growth factor (EGF), and fibroblast growth factor (FGF) (20 ng/mL) (both from Peprotech). Cells were grown to subconfluence, dissociated by Accutase (Thermo Fisher Scientific), and grown ether as neurospheres or as a monolayer on polyornithine- (Sigma) and laminin-coated (Biolamina) plastic.

Western Blot and Co-immunoprecipitation

Cells were lysed in buffer containing 20 mM Tris (pH 8), 150 mM NaCl, 1 mM EDTA, and 0.5% NP40 following co-immunoprecipitation using Dynabeads protein G (Invitrogen) according to the manufacturer's instructions. For western blots, cells were lysed in RIPA buffer supplemented with Complete protease inhibitor cocktail (Roche). The following antibodies were used: C-terminal CD44 (Abcam ab157107), HIF-1α (Novus Biologicals NB100-479), HIF-2α (Abcam ab199), SDHA (Abcam ab14715), actin (Abcam ab75186), HA (Millipore 04-902 and Abcam ab9110), GFP (Abcam ab290 and Abcam ab38689), ADAM10 (Abcam ab1997), ADAM17 (LSbio LS-B619-50), HIFAN (Abcam ab187524). All data represent at least three independent experiments.

Real-Time qPCR

RNA was isolated in using the RNeasy Mini Kit together with the Qiashredder Kit (QIAGEN), and cDNA was synthesized using random primers and MultiScribe reverse transcriptase enzyme (Applied Biosystems). The amplifications were run using a QuantStudio 7 real-time PCR system (Applied Biosystems) with SYBR Green Master Mix (Applied Biosystems). Relative gene expression was normalized to the expression of three housekeeping genes (*UBC*, *SDHA*, and *YWHAZ*) using the comparative Ct method (Vandesompele et al., 2002). All detections were performed in triplicate using the following primers: ADM (human) forward (f): 5′-CACATGATTCTGGAACAGAG-3′, reverse (r): 5′-GTTGTTAAGTTTGTCCCCAG-3′; ADAM10 (human) f: 5′-CACATGATTCTGGAACAGAG-3′ r: 5′-GTTGTTAAGTTTGTCCCCAG-3′; ADAM17 (human) f: 5′-CCATAGCTGTGAGTGGCGAT-3′ r: 5′-TGGGCCTTACTTTCAATGGTCT-3′; BNIP3 (human) f: 5′-AAAATATTCCCCCCAAGGAGTTC-3′, r: 5′-ACGCTCGTGTTCCTCATGCT-3′; CD44 (human) f: 5′-TGGCATCCCTCTTGGCCTTGG-3′,

r: 5′-TGAGACTTGCTGGCCTCTCCGT-3′; Cd44 (mouse) f: 5′- TCGTTGCCC TTCTCCCCACGA-3′, r: 5′-CCTGCGTAGCGGCAGGTTACA-3′; BHLHE40 (human) f: 5′-CAGTGGCTATGGAGGAGAATCG-3′, r: 5′-GCGTCCGTGGTCAC TTTTG-3′; MXI1(human) f: 5′-AGAGGAGATTGAAGTGGATG-3′, r: 5′-CTGGGT TCTATGAAGTGAATG-3′; NANOG (human) f: 5′-GCTGGTTGCCTCATGTT ATTATGC-3′, r: 5′-CCATGGAGGAAGGAAGAGGAGAGA-3′; OCT4 (human) f: 5′-AGCAAAACCCGGAGGAGT-3′, r: 5′-CCACATCGGCCTGTGTATATC-3′; SDHA (human) f: 5′-TGGGAACAAGAGGGCATCTG-3′, r: 5′-CCACCACTG CATCAAATTCATG-3′; Sdha (mouse) f: 5′- CTTGAATGAGGCTGACTG-3′, r: 5′- ATCACATSSGCTGGTCCTG-3′; SOX2 (human) f: 5′- GCCTGGGCGCC GAGTGGA-3′, r: 5′- GGGCGAGCCGTTCATGTAGGTCTG-3′; UBC (human) f: 5′- ATTTGGGTCGCGGTTCTT-3′, r: 5′- TGCCTTGACATTCTCGATGGT-3′; Ubc (mouse) f: 5′- AGCCCAGTGTTACCACCAA −3′, r: 5′- ACCCAAGAACA AGCACAA-3′; YWHAZ (human) f: 5′-ACTTTTGGTACATTGTGGCTTCAA-3′, r: 5′- CCGCCAGGACAAACCAGTAT −3′; Ywhaz (mouse) f: 5′-CAGTAGATG GAGAAAGATTTGC-3′, r: 5′-GGGACAATTAGGGAAGTAAGT-3′.

Side Population Assay

For SP, cells were resuspended at 1 × 10^6 cells/mL and incubated at 37°C, 30 min with or without fumitremorgin C (FTC) (Sigma). Cells were incubated for a further 90 min with 5 mg/mL Hoechst 33342 (Sigma) with periodic shaking. Cells were analyzed on an FACSVerse instrument (BD) equipped with a 405-nm violet laser. Dual-wavelength detection was performed using 448/45 (Hoechst 33342-blue) and 613/18 (Hoechst 33342-red) filters. Data were analyzed using FlowJo software.

Luciferase Assays and Plasmids

For the luciferase reporter assay, cells were co-transfected with HRE-luc (Emerling et al., 2008) (a gift from Navdeep Chandel, Addgene 26731) and pCMV-renilla (Promega) and then analyzed for luciferase using the Dual-Luciferase Reporter Assay System (Promega) on a Synergy 2 plate reader (BioTek). The human pEGFP-CD44ICD plasmid was previously described (Pietras et al., 2014). pcDNA3 was from Invitrogen. The human Notch1-ICD plasmid was a kind gift from J.C. Aster (Aster et al., 1997). pEGFP-C1 was from Clontech Laboratories. O_2-insensitive mutants of *HIF1A* (HIF-1A-2M) and *HIF2A* (HIF-2A-2M) were a gift from William Kaelin (Addgene plasmids 18955 and 18956, respectively) (Emerling et al., 2008; Yan et al., 2007). O_2-insensitive mutant HIF-1A-3M was generated by site directed mutagenesis of Asn803 to- Ala from the *HIF1A* using QuickChange Lightning Site Specific Mutagenesis kit (Agilent). All plasmids were verified by sequencing.

Sphere Formation and Proliferation Assay

For sphere formation, U3065MG cells were plated at single-cell density in 30-μL drops on the lid of a 48-well plate and grown for 7–10 days with 20 μM TAPI-2. Pictures were acquired with an Axio Vert.A1 Zeiss microscope, and sphere area was measured using ImageJ and presented relative to control. For proliferation, U3065MG cells were cultured as monolayer cultures in laminin-coated 6-well plates. 50,000 cells were plated and grown at either 21% or 1% O_2, treated with control or 20 μM TAPI-2, and counted in a hemocytometer at the indicated time points.

Bioinformatic Analysis

Level 3 RNA-sequencing data containing mRNA gene-level RNA-seq by expectation maximization (RSEM) estimates were downloaded from TCGA data portal https://tcga-data.nci.nih.gov/tcga/dataAccessMatrix.htm by September 2014. Gene expression levels for were created by multiplying the gene-level RSEM estimate values by 10^6 followed by adding an offset of 1 and subsequent log2 transformation. The primary tumor from each patient was used, resulting in a dataset comprising 155 samples. Hypoxia pathway activity was estimated for each sample by calculating the mean expression value for genes within the Broad Molecular Signature Database (MSigDB) hypoxia hallmark gene set "HALLMARK_HYPOXIA v5.1" (http://software.broadinstitute.org/gsea/msigdb/index.jsp).

Data from the Allen Institute for Brain Science Ivy Glioblastoma Atlas Project (available at http://glioblastoma.alleninstitute.org) were analyzed using the GlioVis data portal for visualization and analysis of brain tumor expression datasets (Bowman et al., 2017).

Statistical Analysis

Unless otherwise stated, all values are presented as mean ± SEM from at least three independent experiments. Statistical significance was calculated using unpaired, two-sided t tests in GraphPad/Prism. Three levels of significance were used (*$p < 0.05$, **$p < 0.01$, and ***$p < 0.01$).

SUPPLEMENTAL INFORMATION

Supplemental Information includes Supplemental Results and four figures and can be found with this article online at http://dx.doi.org/10.1016/j.celrep.2017.07.049.

AUTHOR CONTRIBUTIONS

A.P., H.A., and E.J. designed the study. E.J., E.S.G., V.P., B.T., T.J.B., D.L., and E.J.P. performed research and analyzed data. A.P., H.A., E.J., E.S.G., V.P., B.T., T.J.B., D.L., and E.J.P. interpreted data. A.P. and E.J. wrote the paper with input from all authors.

ACKNOWLEDGMENTS

We thank Christina Möller for skillful technical assistance and the HGCC project (Xie et al., 2015) for primary GBM cells. This work was supported by grants from the Swedish Research Council, the Ragnar Söderberg Foundation, the Swedish Childhood Cancer Foundation, the Swedish Cancer Society, Ollie & Elof Ericssons Foundation, Jeanssons stiftelser, the Gyllenstierna Krapperup's Foundation, Gunnar Nilssons cancerstiftelse, the Segerfalk Foundation, the Crafoord Foundation, Gösta Miltons minnesfond, the Mary Beve Foundation, and Magnus Bergvalls stiftelse.

Received: February 14, 2017
Revised: May 10, 2017
Accepted: July 19, 2017
Published: August 15, 2017

REFERENCES

Anido, J., Sáez-Borderías, A., Gonzàlez-Juncà, A., Rodón, L., Folch, G., Carmona, M.A., Prieto-Sánchez, R.M., Barba, I., Martínez-Sáez, E., Prudkin, L., et al. (2010). TGF-β receptor inhibitors target the CD44(high)/Id1(high) glioma-initiating cell population in human glioblastoma. Cancer Cell *18*, 655–668.

Aster, J.C., Robertson, E.S., Hasserjian, R.P., Turner, J.R., Kieff, E., and Sklar, J. (1997). Oncogenic forms of NOTCH1 lacking either the primary binding site for RBP-Jkappa or nuclear localization sequences retain the ability to associate with RBP-Jkappa and activate transcription. J. Biol. Chem. *272*, 11336–11343.

Bar, E.E., Lin, A., Mahairaki, V., Matsui, W., and Eberhart, C.G. (2010). Hypoxia increases the expression of stem-cell markers and promotes clonogenicity in glioblastoma neurospheres. Am. J. Pathol. *177*, 1491–1502.

Bleau, A.M., Hambardzumyan, D., Ozawa, T., Fomchenko, E.I., Huse, J.T., Brennan, C.W., and Holland, E.C. (2009). PTEN/PI3K/Akt pathway regulates the side population phenotype and ABCG2 activity in glioma tumor stem-like cells. Cell Stem Cell *4*, 226–235.

Bowman, R.L., Wang, Q., Carro, A., Verhaak, R.G., and Squatrito, M. (2017). GlioVis data portal for visualization and analysis of brain tumor expression datasets. Neuro-oncol. *19*, 139–141.

Bracken, C.P., Fedele, A.O., Linke, S., Balrak, W., Lisy, K., Whitelaw, M.L., and Peet, D.J. (2006). Cell-specific regulation of hypoxia-inducible factor (HIF)-1alpha and HIF-2alpha stabilization and transactivation in a graded oxygen environment. J. Biol. Chem. *281*, 22575–22585.

Brennan, C.W., Verhaak, R.G., McKenna, A., Campos, B., Noushmehr, H., Salama, S.R., Zheng, S., Chakravarty, D., Sanborn, J.Z., Berman, S.H., et al.; TCGA Research Network (2013). The somatic genomic landscape of glioblastoma. Cell *155*, 462–477.

Carpenter, A.E., Jones, T.R., Lamprecht, M.R., Clarke, C., Kang, I.H., Friman, O., Guertin, D.A., Chang, J.H., Lindquist, R.A., Moffat, J., et al. (2006).

CellProfiler: image analysis software for identifying and quantifying cell phenotypes. Genome Biol. *7*, R100.

Cho, H., and Kaelin, W.G. (2016). Targeting HIF2 in Clear Cell Renal Cell Carcinoma. Cold Spring Harb. Symp. Quant. Biol. *81*, 113–121.

Emerling, B.M., Weinberg, F., Liu, J.L., Mak, T.W., and Chandel, N.S. (2008). PTEN regulates p300-dependent hypoxia-inducible factor 1 transcriptional activity through Forkhead transcription factor 3a (FOXO3a). Proc. Natl. Acad. Sci. USA *105*, 2622–2627.

Golebiewska, A., Bougnaud, S., Stieber, D., Brons, N.H., Vallar, L., Hertel, F., Klink, B., Schröck, E., Bjerkvig, R., and Niclou, S.P. (2013). Side population in human glioblastoma is non-tumorigenic and characterizes brain endothelial cells. Brain *136*, 1462–1475.

Hambardzumyan, D., and Bergers, G. (2015). Glioblastoma: defining tumor niches. Trends Cancer *1*, 252–265.

Heddleston, J.M., Li, Z., McLendon, R.E., Hjelmeland, A.B., and Rich, J.N. (2009). The hypoxic microenvironment maintains glioblastoma stem cells and promotes reprogramming towards a cancer stem cell phenotype. Cell Cycle *8*, 3274–3284.

Holland, E.C., Hively, W.P., DePinho, R.A., and Varmus, H.E. (1998). A constitutively active epidermal growth factor receptor cooperates with disruption of G1 cell-cycle arrest pathways to induce glioma-like lesions in mice. Genes Dev. *12*, 3675–3685.

Holmquist-Mengelbier, L., Fredlund, E., Löfstedt, T., Noguera, R., Navarro, S., Nilsson, H., Pietras, A., Vallon-Christersson, J., Borg, A., Gradin, K., et al. (2006). Recruitment of HIF-1alpha and HIF-2alpha to common target genes is differentially regulated in neuroblastoma: HIF-2alpha promotes an aggressive phenotype. Cancer Cell *10*, 413–423.

Huse, J.T., and Holland, E.C. (2010). Targeting brain cancer: advances in the molecular pathology of malignant glioma and medulloblastoma. Nat. Rev. Cancer *10*, 319–331.

Li, Z., Bao, S., Wu, Q., Wang, H., Eyler, C., Sathornsumetee, S., Shi, Q., Cao, Y., Lathia, J., McLendon, R.E., et al. (2009). Hypoxia-inducible factors regulate tumorigenic capacity of glioma stem cells. Cancer Cell *15*, 501–513.

Nagano, O., and Saya, H. (2004). Mechanism and biological significance of CD44 cleavage. Cancer Sci. *95*, 930–935.

Okamoto, I., Kawano, Y., Murakami, D., Sasayama, T., Araki, N., Miki, T., Wong, A.J., and Saya, H. (2001). Proteolytic release of CD44 intracellular domain and its role in the CD44 signaling pathway. J. Cell Biol. *155*, 755–762.

Ozawa, T., Riester, M., Cheng, Y.K., Huse, J.T., Squatrito, M., Helmy, K., Charles, N., Michor, F., and Holland, E.C. (2014). Most human non-GCIMP glioblastoma subtypes evolve from a common proneural-like precursor glioma. Cancer Cell *26*, 288–300.

Pietras, A., Gisselsson, D., Ora, I., Noguera, R., Beckman, S., Navarro, S., and Påhlman, S. (2008). High levels of HIF-2alpha highlight an immature neural crest-like neuroblastoma cell cohort located in a perivascular niche. J. Pathol. *214*, 482–488.

Pietras, A., Johnsson, A.S., and Påhlman, S. (2010). The HIF-2α-driven pseudo-hypoxic phenotype in tumor aggressiveness, differentiation, and vascularization. Curr. Top. Microbiol. Immunol. *345*, 1–20.

Pietras, A., Katz, A.M., Ekström, E.J., Wee, B., Halliday, J.J., Pitter, K.L., Werbeck, J.L., Amankulor, N.M., Huse, J.T., and Holland, E.C. (2014). Osteopontin-CD44 signaling in the glioma perivascular niche enhances cancer stem cell phenotypes and promotes aggressive tumor growth. Cell Stem Cell *14*, 357–369.

Seidel, S., Garvalov, B.K., Wirta, V., von Stechow, L., Schänzer, A., Meletis, K., Wolter, M., Sommerlad, D., Henze, A.T., Nistér, M., et al. (2010). A hypoxic niche regulates glioblastoma stem cells through hypoxia inducible factor 2 alpha. Brain *133*, 983–995.

Semenza, G.L. (2012). Hypoxia-inducible factors: mediators of cancer progression and targets for cancer therapy. Trends Pharmacol. Sci. *33*, 207–214.

Shih, A.H., Dai, C., Hu, X., Rosenblum, M.K., Koutcher, J.A., and Holland, E.C. (2004). Dose-dependent effects of platelet-derived growth factor-B on glial tumorigenesis. Cancer Res. *64*, 4783–4789.

Singh, S.K., Clarke, I.D., Terasaki, M., Bonn, V.E., Hawkins, C., Squire, J., and Dirks, P.B. (2003). Identification of a cancer stem cell in human brain tumors. Cancer Res. *63*, 5821–5828.

Soeda, A., Park, M., Lee, D., Mintz, A., Androutsellis-Theotokis, A., McKay, R.D., Engh, J., Iwama, T., Kunisada, T., Kassam, A.B., et al. (2009). Hypoxia promotes expansion of the CD133-positive glioma stem cells through activation of HIF-1alpha. Oncogene *28*, 3949–3959.

Vandesompele, J., De Preter, K., Pattyn, F., Poppe, B., Van Roy, N., De Paepe, A., and Speleman, F. (2002). Accurate normalization of real-time quantitative RT-PCR data by geometric averaging of multiple internal control genes. Genome Biol. *3*, RESEARCH0034.

Wee, B., Pietras, A., Ozawa, T., Bazzoli, E., Podlaha, O., Antczak, C., Westermark, B., Nelander, S., Uhrbom, L., Forsberg-Nilsson, K., et al. (2016). ABCG2 regulates self-renewal and stem cell marker expression but not tumorigenicity or radiation resistance of glioma cells. Sci. Rep. *6*, 25956.

Xie, Y., Bergström, T., Jiang, Y., Johansson, P., Marinescu, V.D., Lindberg, N., Segerman, A., Wicher, G., Niklasson, M., Baskaran, S., et al. (2015). The human glioblastoma cell culture resource: validated cell models representing all molecular subtypes. EBioMedicine *2*, 1351–1363.

Yan, Q., Bartz, S., Mao, M., Li, L., and Kaelin, W.G., Jr. (2007). The hypoxia-inducible factor 2alpha N-terminal and C-terminal transactivation domains cooperate to promote renal tumorigenesis in vivo. Mol. Cell. Biol. *27*, 2092–2102.